Two-Level System as a Quantum Sensor for Absolute Calibration of Power

T. Hönigl-Decrinis,[1,2,*] R. Shaikhaidarov,[1,3] S.E. de Graaf,[2] V.N. Antonov,[1,3,4] and O.V. Astafiev[1,2,3,4]

[1] *Physics Department, Royal Holloway, University of London, Egham TW20 0EX, United Kingdom*
[2] *National Physical Laboratory, Teddington TW11 0LW, United Kingdom*
[3] *Moscow Institute of Physics and Technology, Dolgoprudny, 141700, Russia*
[4] *Skolkovo Institute of Science and Technology, Nobel Street 3, Moscow, 143026, Russia*

(Received 20 May 2019; revised manuscript received 22 November 2019; accepted 17 January 2020; published 25 February 2020)

A two-level quantum system can absorb or emit not more than one photon at a time. Using this fundamental property, we demonstrate how a superconducting quantum system strongly coupled to a transmission line can be used as a sensor of the photon flux. We propose four methods of sensing the photon flux and analyze them for the absolute calibration of power by measuring spectra of scattered radiation from the two-level system. This type of sensor can be tuned to operate in a wide frequency range, and does not disturb the propagating waves when not in use. Use of a two-level system as a power sensor enables a range of applications in quantum technologies, here in particular applied to calibrate the attenuation of transmission lines inside dilution refrigerators.

DOI: 10.1103/PhysRevApplied.13.024066

I. INTRODUCTION

Progress in development of superconducting circuits, in particular applications in quantum optics, quantum computing, and quantum information, requires calibration of microwave lines and knowledge of powers applied to the circuits situated on a chip at millikelvin temperatures. Usually, one resorts to room-temperature characterization with power meters and spectral analyzers based on semiconductor electronics. However, when the setup including several microwave components (wiring, attenuators, circulators, amplifiers, etc.) is cooled to millikelvin temperatures, their transfer functions are changed. Furthermore, the circuits on the chip are usually omitted from room-temperature characterizations.

There have been several proposals to tackle this problem; for instance, using Planck spectroscopy [1,2], the shot noise of a known microwave component [3], or the scattering parameters of a device under test compared with a reference transmission line [4–6]. These methods may require separate cooldowns or multiple switched cryogenic standards, increasing the measurement time and uncertainty due to unavoidable change of parameters when the microwave lines are reassembled. In experiments with superconducting qubits or resonators, some physical effect specific to the circuit is often used for calibration purposes. For example, photon numbers have been accurately calibrated through the cross-Kerr-effect [7] or via the Stark shift of a qubit-cavity system [8,9]. The latter has been extended to multilevel quantum systems (qudits) to deduce the unknown signal frequency and amplitude from the higher-level ac Stark shift [10]. Another method uses a phase qubit as a sampling oscilloscope by measuring how the flux bias evolves in time [11]. Other approaches are suitable for correcting pulse imperfections [12,13]. An interesting recent proposal uses a transmon qubit coupled to a readout resonator to characterize qubit control lines in the range from 8 to 400 MHz *in situ*. Unfortunately it is limited by the decoherence time of the qubit [14].

In this paper, we present a quantum sensor of absolute power operating in the microwave range and at cryogenic temperatures based on a two-level system in a transmission line. This sensor measures the photon rate (propagated radiation) over a wide frequency range by tuning the two-level system. Importantly, the sensor itself does not disturb the transmission line when detuned. The sensor can be inserted as an additional lossless element into the transmission line close to the reference plane of another device of interest or can be used for calibration of transmission lines, microwave components, or devices within dilution refrigerators. The working principle is independent of the two-level system used, its implementation, and dephasing to first order. We implement the absolute-power quantum sensor using a superconducting flux qubit [15] strongly coupled to a one-dimensional transmission line [7,16–19], but in principle it can be implemented with any two-level system as long as it satisfies the strong-coupling condition. We demonstrate several methods for

*teresa.hoenigl-decrinis@npl.co.uk

measuring the absolute power, the fastest relying on the concept of continuous-wave mixing [20,21]. The accuracy of each method is evaluated by comparing the absolute power sensed at the same frequency by four different qubits on the same chip.

II. DEVICE AND WORKING PRINCIPLE

Our quantum sensor relies on the principle that when a two-level system is illuminated by coherent electromagnetic waves $V_0 e^{-i\omega t}$ with incident photon rate ν, only a fraction of the incident photons are absorbed with rate Ω. As illustrated in Fig. 1(a), the incident electromagnetic wave couples to the two-level system via the dipole interaction energy, $\hbar\Omega = \mu V_0$, where μ is the dipole moment and V_0 is the voltage amplitude of the microwave signal we aim to sense. The incident photon rate is given by $\nu = V_0^2/(2Z\hbar\omega)$, where Z is the impedance of the transmission line that guides the microwave photons to the two-level system at angular frequency ω.

We start with the ideal case of strong coupling of a two-level artificial atom to a one-dimensional transmission line, where nonradiative relaxation is negligible. Insertion of the expression for the relaxation rate $\Gamma_1 = (\mu^2\omega Z)/\hbar$ [18,22] gives

$$\nu = \frac{\Omega^2}{2\Gamma_1}. \tag{1}$$

To sense the incident power $W_0 = \nu\hbar\omega$, we need to find two parameters: the Rabi frequency, Ω, and the relaxation rate, Γ_1 (or μ). These two quantities may be measured independently (e.g., two separate measurements) as the relaxation rate Γ_1 (or the dipole moment μ) is a property of the sensor presented, whereas the Rabi frequency Ω relates to the quantity sensed.

We study different methods of finding the required quantities Ω and Γ_1: (i) by probing the two-level system for reflection through the transmission line, (ii) quantum oscillations, (iii) the Mollow triplet, and (iv) wave mixing [23]. Fig. 1(a) shows the cryogenic environment only, but each method requires somewhat different experimental setups at room temperature. Even though we try to keep the total attenuation similar, there are some variations across the methods.

For this reason, we benchmark our absolute-power sensor at 7.48 GHz, to which we can tune each of the four flux qubits with different parameters available for comparison in our device. As seen in Fig. 1(b), each flux qubit consists of an Al superconducting loop and four $Al/AlO_x/Al$ Josephson junctions fabricated on a silicon oxide substrate, where one of the Josephson junctions, the α junction, has geometrical overlap reduced by a factor of α [20]. The coupling capacitance C_c to the one-dimensional transmission line and the α junction is varied; two qubits are designed to have a coupling capacitance of $C_c = 3$ fF with $\alpha = 0.5$, while the remaining two qubits have $C_c = 5$ fF and $\alpha = 0.45$. All qubits are cofabricated on one sample chip by electron-beam lithography and a shadow evaporation technique with controllable oxidation.

Importantly, with the coupling capacitances $C_c \leq 5$ fF at 7.5 GHz, the reflection is negligible when the qubits are detuned from the resonance. The reflected power W_r on the two-level system from the propagated microwave of power W_0 is given by $W_r/W_0 = (\omega C_c Z_0/2)^2$, here resulting in $W_r < 3 \times 10^{-5} W_0$, and the transmission line can then be regarded as being a low-loss and well-matched 50-Ω line.

The qubits held at 12 mK are revealed through transmission spectroscopy as seen in Fig. 2(a). Although, by design, two in four qubits should be identical (apart from their transmission spectrum in a magnetic field, since their loop area is varied), a clear spread of energies is visible due to technological limitations. We fit numerical simulations for each qubit to the shape of the transition frequency [Fig. 2(b)].

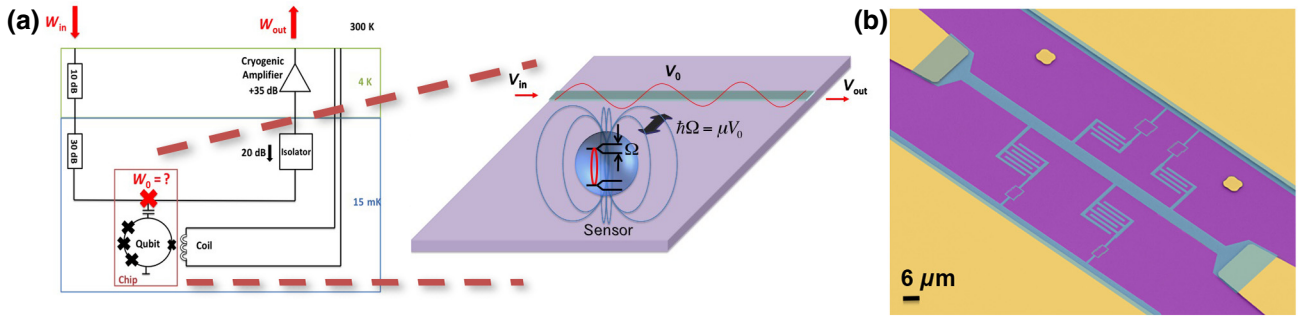

FIG. 1. (a) Schematic of a cryogenic environment together with an illustration of the chip containing a two-level system—the absolute-power quantum sensor—coupled to a transmission line. Knowledge of the absolute power W_0 supplied to a chip at cryogenic temperatures is important for most quantum technologies with superconducting circuits. The two-level system with dipole moment μ interacts with the field V_0 containing many photons, giving rise to coherent oscillations at the Rabi frequency Ω. (b) False-color SEM image of the sample chip featuring four Al (blue) flux qubits on the undoped silicon oxide substrate (violet) and Au ground planes, markers, and bonding pads (yellow).

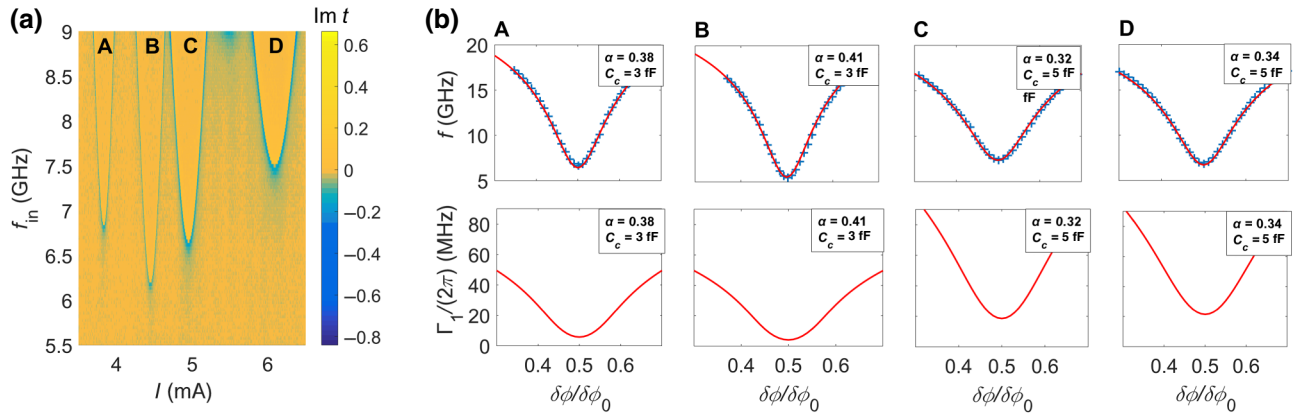

FIG. 2. (a) Transmission spectrum, Im t, of four flux qubits as a function of incident microwave frequency $f_{\rm in}$ and current I through an external superconducting coil providing the bias flux ϕ_b. The transition frequencies are revealed as dips in the transmission spectrum. We benchmark the absolute-power sensor at 7.48 GHz. (b) Transition frequencies f (top row) and relaxation rates (bottom row) $\Gamma_1/(2\pi)$ as a function of flux $\delta\phi/\phi_0$ of artificial atoms A, B, C, and D, where ϕ_0 is the flux quantum and $\delta\phi = \phi_b - \phi_0/2$. Blue markers are experimental points taken from the transmission spectrum. The solid lines are numerical simulations calculated with charging energy $E_C/h = (2e)^2/(2C_J h) = 10$ GHz (with junction capacitance C_J) and Josephson energy $E_J/h = 53$ GHz, with α and coupling capacitance C_c shown in the insets.

To characterize the sensors' relaxation rates, we adjust the external field to tune each qubit to 7.48 GHz. We drive and read out the qubit with energy splitting $\hbar\omega_a$ using a vector network analyzer (VNA). The qubit driven by a microwave tone $V_0 e^{-i\omega t}$ can be described in the rotating-wave approximation by the Hamiltonian $H = (\hbar\delta\omega/2)\sigma_z - (\hbar\Omega/2)\sigma_x$, where $\delta\omega = \omega - \omega_a$ is the detuning from the resonance of the qubit and σ_i are the Pauli matrices. The dynamics of the system is well described by the master equation $\dot{\rho} = -i/\hbar[H,\rho] + \hat{L}[\rho]$, with the Lindblad term $\hat{L}[\rho] = -\Gamma_1\sigma_z\rho_{11} - \Gamma_2(\sigma^+\rho_{10} + \sigma^-\rho_{01})$, where Γ_2 is the dephasing rate. When the artificial two-level atom is driven close to its resonance, it acts as a scatterer and generates two coherent waves propagating forward and backward with respect to the driving field [18]:

$$V_{\rm sc}(x,t) = i\frac{\hbar\Gamma_1}{\mu}\langle\sigma^-\rangle\, e^{ik|x|-i\omega t}, \tag{2}$$

where $\langle\sigma^-\rangle = \rho_{10}$ is found from the stationary solution of the master equation. We measure transmission coefficients $t = 1 + V_{\rm sc}/V_0$, where V_0 and $V_{\rm sc}$ are voltage amplitudes of the incident and scattered electromagnetic waves, respectively [18,19]. We detect the qubit resonances as a sharp dip in the power-transmission coefficient $|t|^2$, and obtain a power extinction $(1 - |t|^2) > 85\%$ for all qubits at 7.48 GHz, confirming strong coupling to the transmission line. In what follows we further assume that the relaxation rate Γ_1 is dominated by the radiative relaxation to the transmission line, an assumption that is justified in the strong-coupling regime.

The reflection coefficient is defined as $V_{\rm sc} = -rV_0$, and using the relation $r = 1 - t$ and Eq. (2), we have [18]

$$r = \frac{\Gamma_1}{2\Gamma_2}\frac{1 + i\delta\omega/\Gamma_2}{1 + (\delta\omega/\Gamma_2)^2 + \Omega^2/\Gamma_1\Gamma_2}. \tag{3}$$

As seen in Eq. (3) [and Fig. 3(a)] the peak in reflection becomes insensitive to driving power at weak driving powers. Fitting the reflection curve in this limit of low driving power, we find the dephasing rate Γ_2 and radiative relaxation rate Γ_1, which are in good agreement with the numerical simulations of each qubit. The results are given in Table I, where the quoted uncertainties (one standard deviation) of Γ_1 and Γ_2 are deduced from the covariance matrix of the fit to the data. Other sources of errors include normalization errors or drifts in frequency due to qubit instability. Frequency fluctuations in state-of-the-art qubits are typically on the scale of kilohertz [24,25]. Here the qubit linewidths are several megahertz, and the contribution of frequency fluctuations of the qubit to the line shape is thus expected to be negligible. Likewise, frequency variations due to instabilities in the flux bias are also negligible as we do not observe any increase in fluctuations for the qubits operated away from their degeneracy points. We normalize the transmission around the qubit resonance by the transmission away from the qubit resonance. This requires tuning of the external magnetic field. Another likely source of error is temporal variations in the power generated and measured by the VNA. This is independently measured to vary by ± 0.25 dB over 1 h (the typical timescale for measurements). This translates to a relative uncertainty in $\Delta r/r = 0.02$ and $\Delta\Gamma_1/\Gamma_1$ of 0.03.

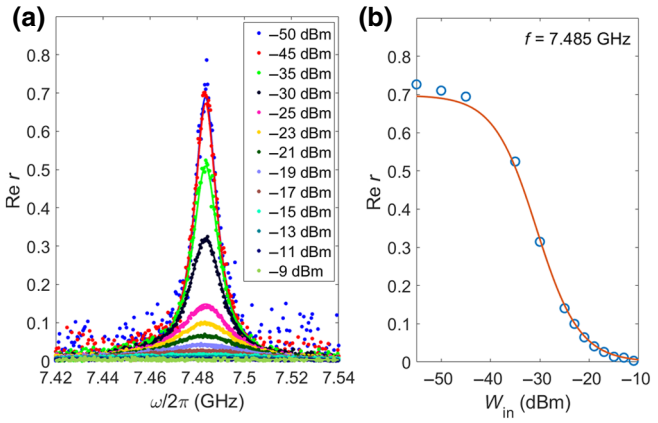

FIG. 3. Qubit A. (a) Reflection as a function of frequency for a set of input powers W_{in}. Markers represent experimental data and solid lines are fits to Eq. (3). (b) Reflection at $f = 7.485$ GHz versus input power W_{in}. Markers represent experimental data and the solid line is a fit.

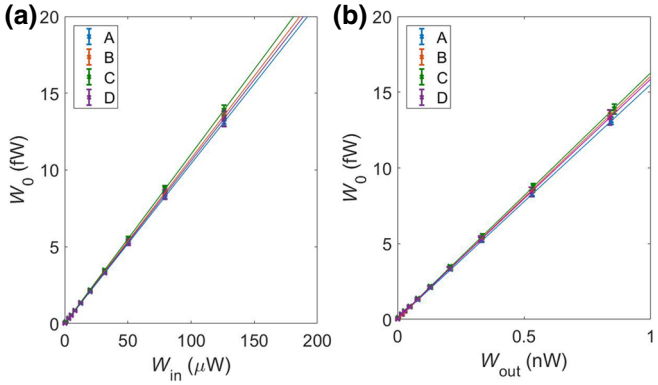

FIG. 4. Absolute power W_0 sensed by qubits A, B, C, and D (Table I) at 7.48 GHz as a function of (a) input power W_{in} and (b) output power W_{out}. The slopes of the linear fits (solid lines) represent (a) attenuation and (b) gain in our measurement circuit.

III. METHODS

Having characterized the four sensors, we now present different methods for measuring the quantity that relates to the power. Because of slightly different experimental setups required at room temperature, we observe slightly different attenuation values across the different methods. We verify that the measured attenuation and gain are in reasonable agreement with the transmission measured through the cryostat at room temperature.

A. Reflection in the transmission line

At $\delta\omega = 0$ the reflection coefficient simplifies to $r = \Gamma_1^2/(2\Gamma_1\Gamma_2 + 2\Omega^2)$, and substitution of the photon rate [Eq. (1)] gives

$$W_0 = \left(\frac{\Gamma_1}{4r} - \frac{\Gamma_2}{2}\right)\hbar\omega. \tag{4}$$

Using a VNA, we measure transmission t around 7.48 GHz for a range of generator input powers W_{in} and deduce the reflection via $r = 1 - t$ for all four qubits as a function of frequency [Fig. 3(a)].

In Fig. 3(b) we plot Re r at $\delta\omega = 0$ versus generator input power W_{in} and fit this curve to Eq. (3) with $\Omega^2 = kW_{\text{in}}$ as the only fitting parameter, where k is an attenuation constant relating the input power to the Rabi frequency. We then calculate the absolute power W_0 according to Eq. (1) (multiplied by $\hbar\omega$). To propagate errors, we take the uncertainty of Γ_1 and Ω from the fits [see Table I and Fig. 3(b), respectively]. These provide the main source of error in sensing the power. Fluctuations in qubit parameters give a negligible contribution.

In Fig. 4 we plot the absolute power W_0 sensed by qubits A, B, C, and D against W_{in} (W_{out}), where the slope represents the attenuation (gain) in our system. We fit this slope for each qubit (see the solid lines in Fig. 4) and find that the attenuation and gain coefficients obtained , listed in Table II, are in agreement within ±0.2 dB, which is comparable to the temporal variations in the measured S_{21} of the VNA, indicating that there is no significant device-dependent systematic error present. Further, the result is consistent with the expected attenuation of approximately 100 dB in this particular measurement setup: in the input line we had placed 90 dB of attenuators and the coaxial

TABLE I. Transition frequency $\omega_0/2\pi$ (at $\delta\phi/\phi_0 = 0.5$), power extinction $1 - |t|^2$, and relaxation and dephasing rates $\Gamma_1/2\pi$ and $\Gamma_2/2\pi$, respectively, at $\omega_a/2\pi = 7.46$ GHz (i.e., $\delta\phi/\phi_0 \neq 0.5$ for qubits A, B, and C) of the four flux qubits (denoted as A, B, C, and D).

Qubit	$\omega_0/2\pi$ (GHz)	$1 - \lvert t\rvert^2$	$\Gamma_1/2\pi$ (MHz)	$\Gamma_2/2\pi$ (MHz)
A	6.83	92%	8.2 ± 0.2	5.7 ± 0.1
B	6.19	87%	7.8 ± 0.2	6.2 ± 0.1
C	6.63	93%	16.4 ± 0.4	10.4 ± 0.2
D	7.46	94%	18.4 ± 0.3	11.6 ± 0.1

TABLE II. Gain and attenuation coefficients obtained from qubits A, B, C, and D for the reflection through the transmission-line method. Errors are propagated from the uncertainties in Γ_1 as listed in Table I and the uncertainties in Ω as extracted from the fit of r as a function of input power W_{in}.

Qubit	Attenuation (dB)	Gain (dB)
A	-99.8 ± 0.2	48.1 ± 0.2
B	-99.7 ± 0.3	48.0 ± 0.3
C	-99.6 ± 0.4	47.9 ± 0.4
D	-99.8 ± 0.4	48.0 ± 0.4
Combined	-99.8 ± 0.2	48.0 ± 0.2

wiring is expected to add roughly 10 dB in attenuation, as verified at room temperature.

Some power may leak from the input to the output of the chip via ground planes or box modes. This power can interfere with the signal, resulting in distortions in the measured reflection curve, or may become apparent as an offset, which is subtracted when we fit the experimental points in Fig. 3(b).

B. Rabi oscillations

An alternative method comprises measuring Ω directly and deducing the absolute power via $W_0 = \hbar\omega\Omega^2/(2\Gamma_1)$. We obtain Ω for a set of driving powers $W_{\rm in}$ by modifying the measurement circuit and performing quantum-oscillation measurements. At the input, an incident microwave pulse is formed with pulse length varying from 1.5 to 15.5 ns to excite the qubit. We perform Rabi-oscillation measurements for all qubits tuned to 7.48 GHz for a range of input microwave powers, $W_{\rm in}$, set at the microwave generator at room temperature. For each input power, we extract the period from fits to the measured Rabi oscillations [Fig. 5(a)]. As expected, we observe a linear relationship between Rabi frequency and driving amplitude. From this fit, we find that the typical uncertainty on the deduced Rabi frequency is ± 10 MHz. This and the uncertainty in Γ_1 are the main sources of error in the measured absolute power.

Figure 5(b) shows the absolute power W_0 sensed by qubits A, B, C, and D (Table I) as a function of input power $W_{\rm in}$. We fit the slope for each qubit individually and find a spread of 0.1 dB in the attenuation coefficients obtained (Table III). We expect the mixers and filters that are added to the experimental setup for the creation of the excitation pulse to contribute around 2.5 dB, measured at room temperature. Taking this additional attenuation into account, we find the attenuation coefficients obtained are also in agreement with the ones extracted with the previous method.

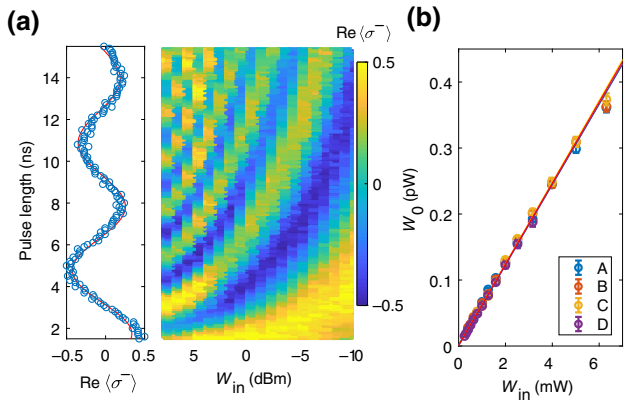

FIG. 5. (a) Rabi oscillations (of qubit B) for input powers $W_{\rm in}$ ranging from -10 to 8 dBm. The inset shows the normalized dipole moment $\langle\sigma^-\rangle$ for input power $W_{\rm in} = -2$ dBm. Blue circles represent experimental data and solid red line is a linear fit. (b) Absolute power W_0 sensed by qubits A, B, C, and D (Table I) at 7.48 GHz as a function of input power $W_{\rm in}$. The slopes of the linear fits (solid lines) represent attenuation in our measurement circuit.

TABLE III. Attenuation coefficients extracted from measuring Rabi oscillations of qubits A, B, C, and D. The uncertainties are obtained by propagating the error in Γ_1 as listed in Table I and the uncertainties in Ω as extracted from the fit of the Rabi oscillations, which constitute the main sources of error for this method.

Qubit	Attenuation (dB)
A	-102.2 ± 0.4
B	-102.2 ± 0.3
C	-102.1 ± 0.4
D	-102.1 ± 0.2
Combined	-102.1 ± 0.2

Disadvantages of this method are that the measurement time of Rabi oscillations is limited by dephasing and that the combinations of mixers forming the pulse can exhibit nonlinear behavior. At high input powers, the oscillations may distort due to interference with leaked power. It may then become necessary to record the power leakage detuned from the qubit to subtract the background, doubling the already-long total measurement time. At relatively low input powers it may not be possible to measure many periods, and the Rabi frequency has to be deduced through linear interpolation.

C. Mollow triplet

A more-robust way to deduce the Rabi frequency Ω is to measure the artificial atom's incoherent spectrum under a strong drive. The two-level system coupled to a strong driving field ($\Omega^2 \gg \Gamma_1^2$) can be described by the dressed-state picture in which the atomic levels are split by Ω. Four transitions between the dressed states are allowed, giving rise to the Mollow or resonance-fluorescence triplet [18,26,27]. The side peaks of the triplet are separated by $2\,\Omega$. To observe the Mollow triplet we measure the power spectrum around 7.48 GHz using a spectrum analyzer under a strong resonant drive (Fig. 6). To resolve the side peaks we rely on many averages, making this the slowest method. The expected spectral density of the incoherent emission is given by [18]

$$S(\omega) \approx \frac{1}{2\pi}\frac{\hbar\omega\Gamma_1}{8}\left(\frac{\gamma_s}{(\delta\omega+\Omega)^2+\gamma_s^2} + \frac{2\gamma_c}{\delta\omega^2+\gamma_c^2} + \frac{\gamma_s}{(\delta\omega-\Omega)^2+\gamma_s^2}\right), \quad (5)$$

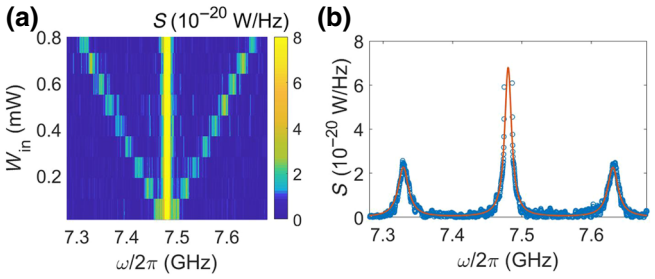

FIG. 6. (a) Mollow triplet (of qubit B) as a function of W_{in} and frequency. (b) Linear frequency spectral density of emission power under a resonant drive with fixed driving power $W_{\text{in}} = 0.73$ mW forming the Mollow triplet. Experimental data are represented by blue circles. The solid red curve is the fit of the emission spectrum according to Eq. (5) with $\Gamma_1 = 7.8$ MHz and $\Gamma_2 = 6.2$ MHz (as in Table I). From the fitting parameters we obtain the Rabi frequency as a function of the external input power.

where the half-widths of the central and side peaks are $\gamma_c = \Gamma_2$ and $\gamma_s = (\Gamma_1 + \Gamma_2)/2$, respectively.

We deduce Ω from fitting the resonance-fluorescence spectrum. The fit gives relative uncertainty $\Delta\Omega/\Omega \leq 0.01$, where $\Delta\Omega$ is the uncertainty of Ω. We calculate the absolute power according to $W_0 = \Omega^2/(2\Gamma_1)\hbar\omega$, where we use the relaxation rates as given in Table I. Again, we plot W_{in} against W_0 and fit it to a straight line for each qubit individually, as seen in Fig. 7. The resulting attenuation coefficients are listed in Table IV. Here the measurement setup at room temperature is the same in terms of the attenuation as the one used for the reflection method. We roughly estimate the gain of the output line in our measurement circuit from the amplitude of the Mollow triplet to be approximately 45 dB. The main factor contributing to the error bars in Fig. 7 is the uncertainty of Γ_1.

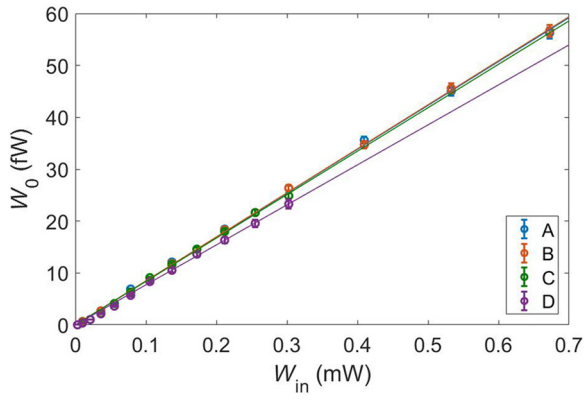

FIG. 7. Absolute power W_0 sensed with use of the Mollow-triplet method by qubits A, B, C, and D (Table I) at 7.48 GHz as a function of input power W_{in}. The slopes of the linear fits (solid lines) represent attenuation in our measurement circuit.

TABLE IV. Line calibration using the Mollow-triplet method. The errors are propagated using the uncertainties in Γ_1 as listed in Table I and the uncertainties in Ω as extracted from the fit of the resonance-fluorescence triplet.

Qubit	Attenuation (dB)	Gain (dB)
A	-100.7 ± 0.1	44 ± 1
B	-100.7 ± 0.1	45 ± 1
C	-100.8 ± 0.1	45 ± 2
D	-101.1 ± 0.1	45 ± 2
Combined	-101.0 ± 0.1	45 ± 2

D. Wave mixing

Some of the methods described above share the potential issue of distortions in the measurements due to interference with leaked power. An elegant solution to this problem is to decouple the input driving powers from the readout signal in the frequency domain.

We drive the artificial atom by two continuous tones with frequencies $\omega_- = \omega_0 - \delta\omega$ and $\omega_+ = \omega_0 + \delta\omega$, where $\omega_0 = 7.48$ GHz and negligible detuning $\delta\omega = 5$ kHz $\ll \Gamma_1$. The mixing processes can be described in terms of multiphoton elastic scattering. For example, a photon at $2\omega_- - \omega_+$ is emitted as a result of absorption of two photons from the ω_- mode and emission of a single photon from the ω_+ mode. Similarly a photon at $2\omega_+ - \omega_-$ is created due to absorption of two photons from the ω_+ mode and emission of a single photon from the ω_- mode. As long as the two driving modes consist of many propagating photons on timescales comparable to the relaxation and dephasing rates Γ_1 and Γ_2, respectively, higher-order processes of wave mixing will be present. As illustrated in Fig. 8, $2p+1$ interacting photons result in spectral components at $\omega_{\pm(2p+1)} = (p+1)\omega_\pm - p\omega_\mp$, where $p \geq 0$ is an integer. An analytical formula for the amplitude of the scattered spectral components is as follows [20]:

$$V^{\text{sc}}_{\pm(2p+1)} = \frac{(-1)^p \Gamma_1 \tan\theta \tan^p \frac{\theta}{2}}{\Lambda} \left(V_\mp \tan\frac{\theta}{2} - V_\pm \right). \quad (6)$$

For equal driving amplitudes $\Omega_+ = \Omega_- = \Omega$, $\theta = \arcsin\left(2\Gamma_2\Omega^2/\Gamma_1|\lambda|^2 + 2\Gamma_2\Omega^2\right)$, and $\Lambda^{-1} = \lambda\Gamma_1/4\Omega^2$, with $\lambda = \Gamma_2 + i\Delta_d$, where Δ_d is detuning from the central frequency.

We denote the spectral components measured at the frequencies of our driving tones as $V'_\pm$ since they consist of the scattered spectral component $V^{\text{sc}}_\pm$ and the driving amplitude $V_\pm$.

Having already characterized relaxation rates Γ_1, we need only to record the amplitudes of the wave-mixing peaks $V'_\pm$ and $V^{\text{sc}}_{\mp 3}$ for a set of powers W_{in}. Since drive and readout signals are decoupled in frequency in this method, we do not need to measure the power leakage detuned from the qubit to subtract the background, significantly decreasing the total measurement time.

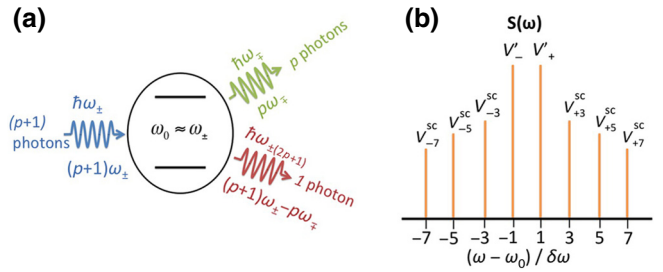

FIG. 8. (a) The mixing processes with $2p+1$ interacting photons on a single artificial atom with transition frequency ω_0 resulting in (b) spectral components $V^{sc}_{\pm(2p+1)}$ at $\omega_{\pm(2p+1)} = \omega_0 \pm (2p+1)\delta\omega$, where $p \geq 0$ is an integer.

As seen in Fig. 9, we measure the spectral components as a function of detuning of the central frequency $\omega_0' = \omega_0 \pm \Delta_d$ while keeping $\delta\omega$, the separation between the two drives $\omega_\pm = \omega_0' \pm \delta\omega$, constant and observe an Autlers-Townes-like splitting. Fitting this splitting to Eq. (6), we extract Ω and its relative uncertainty $\Delta\Omega/\Omega < 0.03$. We calculate the absolute power W_0 according to Eq. (1). Again, we propagate the errors using the uncertainties in the relaxation rate Γ_1, as listed in Table I, and the relative uncertainty $\Delta\Omega/\Omega$ as found from the covariance matrix of the fit to the Autlers-Townes-like splitting.

To measure the mixing it is necessary to modify the experimental setup at room temperature and include a microwave combiner, leading to a slightly a higher measured attenuation of approximately 3 dB, see Table V, compared with the reflection or Mollow-triplet method. We obtain attenuation and gain coefficients for each sensor with a spread of 0.2 dB by the data fitting to a straight line (Table V, Fig. 10).

Finally, the total measurement time can be significantly decreased by measuring a single slice at $\Delta_d = 0$. We introduce the variables $\alpha_m = V^{sc}_{\mp3}/V'_\pm$ and $x = \Gamma_1/\Omega$ at the exact resonance when $\Delta_d = 0$. We set $\Gamma_2/\Gamma_1 = \chi$, which has minimal value 1/2 in the absence of pure dephasing. Using the variables, we now express the photon-emission rate as $\nu = (\Gamma_1/2)x^{-2}$. With Eq. (6) we expand α_m in series, $\alpha_m = x^2/4 + o(x^3)$, and therefore $x^{-2} = 1/4\alpha_m + o(\alpha_m^{3/2})$ and $\nu = (\Gamma_1/8\alpha_m)\eta$, where $\eta = 1 - 3\sqrt{\chi\alpha_m} + (1-\chi/2)\alpha_m + o(\alpha_m^{3/2})$. To first order the photon-emission rate,

$$\nu_1 = \frac{\Gamma_1}{8}\frac{V'_\pm}{V^{sc}_{\mp3}}, \tag{7}$$

does not contain a dephasing term (χ). To correct for higher orders, ν_1 is multiplied by the correction term η, such that $\nu = \nu_1\eta$.

For example, for $\alpha_m = 10^{-4}$, the approximation of Eq. (7) gives the result with an accuracy of approximately $\sqrt{\alpha_m}$, which is about 2%. Accounting for the correction terms will reduce the derivation error to approximately $\alpha_m^{3/2} \approx 10^{-6}$. Using this simplified method, we can arrive at attenuation and gain values with errors of the same magnitude as for the other methods within minutes, greatly reducing the total measurement time.

TABLE V. Attenuation coefficients extracted from measuring wave mixing of qubits A, B, C, and D. The errors are propagated using the uncertainties in Γ_1 as listed in Table I and the uncertainties in Ω as extracted from the fit of the Autler-Townes-like splitting of the spectral components of the first-order side peak [Fig. 10(b)].

Qubit	Attenuation (dB)	Gain (dB)
A	-102.0 ± 0.1	44.9 ± 0.1
B	-102.1 ± 0.2	45.0 ± 0.2
C	-101.9 ± 0.4	44.8 ± 0.4
D	-101.8 ± 0.3	44.8 ± 0.3
Combined	-102.0 ± 0.1	44.9 ± 0.1

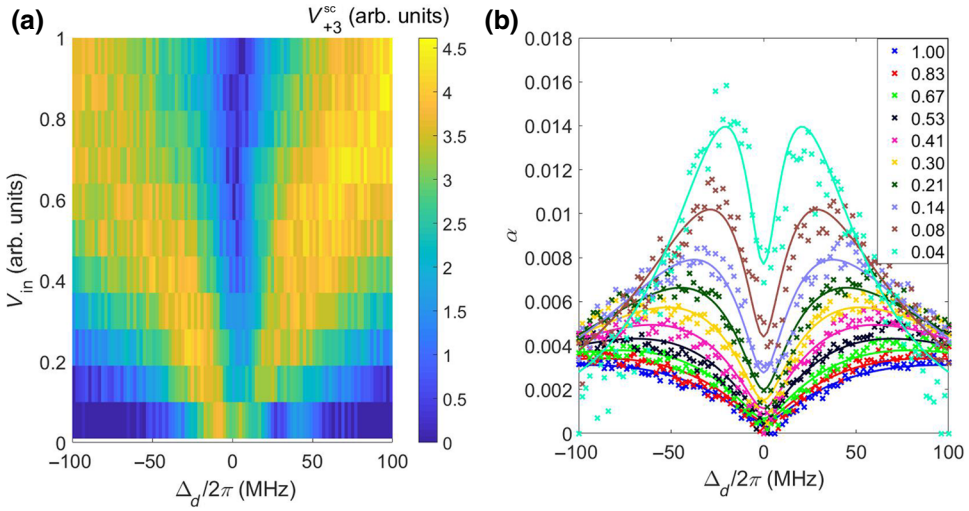

FIG. 9. Qubit A. (a) Autler-Townes-like splitting of the spectral component of the first-order ($p = 1$) side peak V^{sc}_{+3}, which appears at $\omega_{+3} = \omega_0' + 3\delta\omega$ due to continuous-wave mixing with two drives of equal amplitudes ranging from 1 to 0.1 $(\mathrm{mW})^{1/2}$. (b) The ratio $\alpha = V^{sc}_{+3}/V'_-$ as a function of detuning Δ_d. The Autlers-Townes-like splitting increases with driving power (arbitrary units). Markers represent experimental points and solid lines are fits.

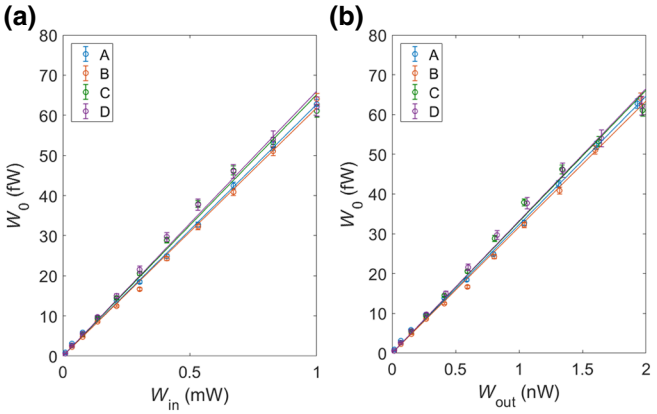

FIG. 10. Mixing method with equal driving powers: The absolute power W_0 sensed by qubits A, B, C, and D (Table I) at 7.48 GHz as a function of (a) input power W_{in} and (b) output power W_{out}. The slope of the linear fit (solid red line) represents (a) attenuation and (b) gain in our measurement circuit.

IV. CONCLUSION

To summarize, we develop an absolute-power quantum sensor based on a superconducting qubit operating in a wide gigahertz range at millikelvin temperatures. Our work addresses the current lack of devices optimized for low-temperature microwave calibration.

We show that the absolute power is determined by two quantities only, the Rabi frequency Ω and the device-dependent relaxation rate Γ_1. The methods presented are based on measuring spectra of scattered radiation through a transmission line; however, the fastest and most-promising technique, from our point of view, relies on a recently demonstrated effect of wave mixing on a quantum system.

For each method, we find that the powers sensed by different qubits with different relaxation rates are in agreement. We do not see qubits with similar relaxation rates group, ruling out significant systematic errors in the measurement of the relaxation rate. We analyze our results for the attenuation and gain in our measurement setup with a spread smaller than 0.4 dB across all methods and find that they are in good agreement with our expectations. Table VI shows a comparison of the average attenuation for each method, where the measured attenuation is adjusted to reflect the difference in attenuation introduced by the slightly different setups for the different methods. The results obtained with the four methods for this scaled attenuation are consistent with one another within approximately 1.4 dB, giving an upper limit to any additional systematic error of any of these methods.

Our sensor does not affect the transmission of microwaves when detuned in frequency, enabling its use in combination with other microwave devices and allowing the sensor to be incorporated on a chip or plugged into the transmission line at a point of interest. We expect this to be useful for applications in quantum-information processing, as well as for fundamental research applications in cryogenic environments.

TABLE VI. Summary of attenuation and gain coefficients of the input and output microwave lines in our dilution refrigerator obtained by the different methods and scaled to the reflection-setup parameters.

Method	Attenuation (dB)	Gain (dB)
Reflection (Sec. III A)	-99.8 ± 0.2	48.0 ± 0.2
Rabi oscillations (Sec. III B)	-99.6 ± 0.5	...
Mollow triplet (Sec. III C)	-101.0 ± 0.1	45 ± 2
Mixing (Sec. III D)	-99.0 ± 0.5	44.9 ± 0.1

ACKNOWLEDGMENTS

We thank A. Dmitriev, J. Burnett, T. Lindström, S. Giblin, and A. Tzalenchuk for helpful discussions. We gratefully acknowledge the UK Department of Business, Energy and Industrial Strategy, the Industrial Strategy Challenge Fund Metrology Fellowships, and the Russian Science Foundation (Grant No. 16-12-00070) for supporting the work.

[1] J. Goetz, S. Pogorzalek, F. Deppe, K. G. Fedorov, P. Eder, M. Fischer, F. Wulschner, E. Xie, A. Marx, and R. Gross, Photon Statistics of Propagating Thermal Microwaves, Phys. Rev. Lett. **118**, 103602 (2017).

[2] M. Mariantoni, E. P. Menzel, F. Deppe, M. A. Araque Caballero, A. Baust, T. Niemczyk, E. Hoffmann, E. Solano, A. Marx, and R. Gross, Planck Spectroscopy and Quantum Noise of Microwave Beam Splitters, Phys. Rev. Lett. **105**, 133601 (2010).

[3] N. Bergeal, F. Schackert, L. Frunzio, D. E. Prober, and M. H. Devoret, Mesoscopic resistor as a self-calibrating quantum noise source, Appl. Phys. Lett. **100**, 203507 (2012).

[4] J.-H. Yeh and S. M. Anlage, In situ broadband cryogenic calibration for two-port superconducting microwave resonators, Rev. Sci. Instrum. **84**, 034706 (2013).

[5] L. Ranzani, L. Spietz, and J. Aumentado, Broadband calibrated scattering parameters characterization of a superconducting quantum interference device amplifier, Appl. Phys. Lett. **103**, 022601 (2013).

[6] L. Ranzani, L. Spietz, Z. Popovic, and J. Aumentado, Two-port microwave calibration at millikelvin temperatures, Rev. Sci. Instrum. **84**, 034704 (2013).

[7] I.-C. Hoi, A. F. Kockum, T. Palomaki, T. M. Stace, B. Fan, L. Tornberg, S. R. Sathyamoorthy, G. Johansson, P. Delsing, and C. M. Wilson, Giant Cross–Kerr Effect for Propagating Microwaves Induced by an Artificial Atom, Phys. Rev. Lett. **111**, 053601 (2013).

[8] D. I. Schuster, A. Wallraff, A. Blais, L. Frunzio, R.-S. Huang, J. Majer, S. M. Girvin, and R. J. Schoelkopf, ac Stark Shift and Dephasing of a Superconducting Qubit

Strongly Coupled to a Cavity Field, Phys. Rev. Lett. **94**, 123602 (2005).

[9] D. I. Schuster, A. A. Houck, J. A. Schreier, A. Wallraff, J. M. Gambetta, A. Blais, L. Frunzio, J. Majer, B. Johnson, M. H. Devoret, S. M. Girvin, and R. J. Schoelkopf, Resolving photon number states in a superconducting circuit, Nature **445**, 515 (2007).

[10] A. Schneider, J. Braumüller, L. Guo, P. Stehle, H. Rotzinger, M. Marthaler, A. V. Ustinov, and M. Weides, Local sensing with the multilevel ac Stark effect, Phys. Rev. A **97**, 062334 (2018).

[11] M. Hofheinz, H. Wang, M. Ansmann, R. C. Bialczak, E. Lucero, M. Neeley, A. D. O'Connell, D. Sank, J. Wenner, J. M. Martinis, and A. N. Cleland, Synthesizing arbitrary quantum states in a superconducting resonator, Nature **459**, 546 (2009).

[12] S. Gustavsson, O. Zwier, J. Bylander, F. Yan, F. Yoshihara, Y. Nakamura, T. P. Orlando, and W. D. Oliver, Improving Quantum Gate Fidelities by Using a Qubit to Measure Microwave Pulse Distortions, Phys. Rev. Lett. **110**, 040502 (2013).

[13] J. Bylander, M. S. Rudner, A. V. Shytov, S. O. Valenzuela, D. M. Berns, K. K. Berggren, L. S. Levitov, and W. D. Oliver, Pulse imaging and nonadiabatic control of solid-state artificial atoms, Phys. Rev. B **80**, 220506 (2009).

[14] M. Jerger, A. Kulikov, Z. Vasselin, and A. Fedorov, In-Situ Characterization of Qubit Control Lines: A Qubit as a Vector Network Analyzer, Phys. Rev. Lett. **123**, 150501 (2019).

[15] J. E. Mooij, T. P. Orlando, L. Levitov, L. Tian, C. H. van der Wal, and S. Lloyd, Josephson persistent-current qubit, Science **285**, 1036 (1999).

[16] O. Astafiev, K. Inomata, A. O. Niskanen, T. Yamamoto, Y. A. Pashkin, Y. Nakamura, and J. S. Tsai, Single artificial-atom lasing, Nature **449**, 588 (2007).

[17] O. V. Astafiev, A. A. Abdumalikov, A. M. Zagoskin, Y. A. Pashkin, Y. Nakamura, and J. S. Tsai, Ultimate On-Chip Quantum Amplifier, Phys. Rev. Lett. **104**, 183603 (2010).

[18] O. Astafiev, A. M. Zagoskin, A. A. Abdumalikov, Y. A. Pashkin, T. Yamamoto, K. Inomata, Y. Nakamura, and J. S. Tsai, Resonance fluorescence of a single artificial atom, Science **327**, 840 (2010).

[19] I.-C. Hoi, C. M. Wilson, G. Johansson, J. Lindkvist, B. Peropadre, T. Palomaki, and P. Delsing, Microwave quantum optics with an artificial atom in one-dimensional open space, New J. Phys. **15**, 025011 (2013).

[20] A. Y. Dmitriev, R. Shaikhaidarov, T. Hönigl-Decrinis, S. E. de Graaf, V. N. Antonov, and O. V. Astafiev, Probing photon statistics of coherent states by continuous wave mixing on a two-level system, Phys. Rev. A **100**, 013808 (2019).

[21] T. Hönigl-Decrinis, I. V. Antonov, R. Shaikhaidarov, V. N. Antonov, A. Y. Dmitriev, and O. V. Astafiev, Mixing of coherent waves in a single three-level artificial atom, Phys. Rev. A **98**, 041801 (2018).

[22] Z. H. Peng, S. E. De Graaf, J. S. Tsai, and O. V. Astafiev, Tuneable on-demand single-photon source in the microwave range, Nat. Commun. **7**, 12588 (2016).

[23] A. Y. Dmitriev, R. Shaikhaidarov, V. N. Antonov, T. Hönigl-Decrinis, and O. V. Astafiev, Quantum wave mixing and visualisation of coherent and superposed photonic states in a waveguide, Nat. Commun. **8**, 1352 (2017).

[24] J. J. Burnett, A. Bengtsson, M. Scigliuzzo, D. Niepce, M. Kudra, P. Delsing, and J. Bylander, Decoherence benchmarking of superconducting qubits, npj Quantum Inf. **5**, 54 (2019).

[25] S. Schlör, J. Lisenfeld, C. Müller, A. Bilmes, A. Schneider, D. P. Pappas, A. V. Ustinov, and M. Weides, Correlating Decoherence in Transmon Qubits: Low Frequency Noise by Single Fluctuators, Phys. Rev. Lett. **123**, 190502 (2019).

[26] B. R. Mollow, Power spectrum of light scattered by two-level systems, Phys. Rev. **188**, 1969 (1969).

[27] M. Baur, S. Filipp, R. Bianchetti, J. M. Fink, M. Göppl, L. Steffen, P. J. Leek, A. Blais, and A. Wallraff, Measurement of Autler-Townes and Mollow Transitions in a Strongly Driven Superconducting Qubit, Phys. Rev. Lett. **102**, 243602 (2009).